Effect of Sodium Sulfide on Ni-Containing Carbon Monoxide Dehydrogenases[†]

Jian Feng [§] and Paul A. Lindahl [§,‡]*

Departments of Chemistry and of Biochemistry and Biophysics, Texas A&M University, College Station, Texas 77843-3255

[†] This work was supported by the National Institutes of Health (GM46441) and the Department of Energy (DE-FG03-01ER15177). The National Science Foundation supported the purchase of the EPR spectrometer (CHE-0092010).

* To whom correspondence should be addressed. Phone: (979) 845-0956. Fax: (979) 845-4719. E-mail: Lindahl@mail.chem.tamu.edu.

[§] Department of Chemistry.

‡ Department of Biochemistry and Biophysics.

Running Title: Effect of Sulfide on CODH

Abstract

The structure of the active-site C-cluster in CO dehydrogenase from *Carboxythermus hydrogenoformans* includes a μ^2-sulfide ion bridged to the Ni and unique Fe, while the same cluster in enzymes from *Rhodospirillum rubrum* ($CODH_{Rr}$) and *Moorella thermoacetica* ($CODH_{Mt}$) lack this ion. This difference was investigated by exploring the effects of sodium sulfide on activity and spectral properties. Sulfide partially inhibited the CO oxidation activity of $CODH_{Rr}$ and generated a lag prior to steady-state. $CODH_{Mt}$ was inhibited similarly but without a lag. Adding sulfide to $CODH_{Mt}$ in the C_{red1} state caused the $g_{av} = 1.82$ EPR signal to decline and new features to appear, including one with g = 1.95, 1.85 and (1.70 or 1.62). Removing sulfide caused the $g_{av} = 1.82$ signal to reappear and activity to recover. Sulfide did not affect the $g_{av} = 1.86$ signal from the C_{red2} state. A model was developed in which sulfide binds reversibly to C_{red1}, inhibiting catalysis. Reducing this adduct causes sulfide to dissociate, C_{red2} to develop, and activity to recover. Using this model, apparent K_I values are 40 ± 10 nM for $CODH_{Rr}$ and 60 ± 30 μM for $CODH_{Mt}$. Effects of sulfide are analogous to those of other anions, including the substrate hydroxyl group, suggesting that these ions also bridge the Ni and unique Fe. This proposed arrangement raises the possibility that CO binding labilizes the bridging hydroxyl and increases its nucleophilic tendency towards attacking Ni-bound carbonyl.

Ni-containing carbon monoxide dehydrogenases are found in anaerobic bacteria and archaea that grow autotrophically on CO or CO_2 and reducing equivalents (*1*). They contain a novel Ni-Fe-S cluster called the *C-cluster* that serves as the active site for the reversible oxidation of CO to CO_2 (reaction [1], where MV refers to the commonly used *in-vitro* electron acceptor/donor methyl viologen).

$$CO + H_2O + 2MV^{2+} \rightleftarrows CO_2 + 2H^+ + 2MV^{1+} \qquad [1]$$

X-ray crystal structures of enzymes from 3 organisms, including *Carboxythermus hydrogenoformans* ($CODH_{Ch}$) *Rhodospirillum rubrum* ($CODH_{Rr}$), and *Moorella thermoacetica* ($CODH_{Mt}$) have been published, including two independent structures for $CODH_{Mt}$ (*2-5*). $CODH_{Ch}$ and $CODH_{Rr}$ are β_2 homodimers with molecular masses of 120 – 140 kDa, while $CODH_{Mt}$ is a 310 kDa $\alpha_2\beta_2$ tetramer. The α subunits of $CODH_{Mt}$ catalyze another reaction not catalyzed by the other two enzymes, namely the synthesis of acetyl-CoA. The four β_2 structures are essentially equivalent, in that each β subunit contains 1 C-cluster and 1 $[Fe_4S_4]^{2+/1+}$ *B-cluster*. Another Fe_4S_4 cubane called the *D-cluster* bridges the two β subunits. B- and D-clusters transfer electrons between the C-cluster and external redox agents.

Reported structures of the C-cluster are similar but not identical. The C-cluster in $CODH_{Ch}$ consists of 1 Ni, 4 Fe, and 5 sulfide ions (Figure 1, left). Three irons and 4 sulfide ions are organized as an $[Fe_3S_4]$ subsite, while the Ni and remaining Fe can be viewed as a [Ni Fe] subsite bridged by a μ^2–bridging sulfide ion. Structures of the other three C-clusters lack this sulfide ion, as shown in Figure 1, right. There are other potentially important differences between these structures but these will not be discussed here.

The C-cluster can be stabilized in four redox states, called C_{ox}, C_{red1}, C_{int} and C_{red2} (*6-9*). The fully-oxidized C_{ox} state is S = 0 and appears not to be involved in CO/CO_2 redox catalysis.

Reduction by 1 electron to the S = ½ C_{red1} state activates the enzyme (*10*). During catalysis, CO probably coordinates to the Ni of the C-cluster in this state, followed by the attack of the carbonyl by a hydroxide ion, forming a Ni-bound carboxylate. The S = ½ C_{red2} state then forms as CO_2 dissociates. The C-cluster in the C_{red2} state transfers 2 electrons, in 1-electron steps, to the B- and D-clusters. In doing so, it passes through an EPR-silent C_{int} state (*9*) and ultimately returns to the C_{red1} state (*7*).

We were intrigued by the μ^2-sulfide ion uniquely found in the $CODH_{Ch}$ C-cluster, and endeavored to understand the circumstances for its presence. One possibility was that this sulfide ion is required for catalysis and that the 3 structures lacking it might reflect enzyme crystallized in an inactive form. Alternatively, the sulfide ion might inhibit catalysis and $CODH_{Ch}$ might have been crystallized in an inactive form. Other possibilities are that the C-cluster in $CODH_{Ch}$ might differ intrinsically from those in the other enzymes, or that the sulfide ion might only bind to a particular C-cluster redox state. In this study, we address these issues by examining the effect of sulfide ion on the activity and spectral properties of $CODH_{Mt}$ and $CODH_{Rr}$. Our results indicate that added sulfide ion *inhibits* catalysis and binds to the C_{red1} state but not to the C_{red2} state of the C-cluster. Implications for the structure of the C-cluster and mechanism of catalysis are discussed.

Experimental Procedures

General Procedures *R. rubrum* and *M. thermoacetica* cells were grown as described (*10,11*). $CODH_{Rr}$ and $CODH_{Mt}$ were purified anaerobically as described (*10-12*). Protein concentrations, CO oxidation activities, electrochemical potential measurements, and stopped-flow experiments were performed as described (*10*). Unless mentioned otherwise, experiments involving protein manipulations were performed in an Ar-atmosphere glove box (Vacuum/Atmosphere) containing less than 1 ppm O_2 as monitored continuously by an analyzer (Teledyne Analytical Instruments,

model 310). EPR experiments were performed using a Bruker EMX spectrometer using ER4116DM (dual mode) and ER4102ST (standard mode) cavities and an Oxford Instruments ESR900 continuous flow cryostat. CO oxidation activities are reported as $\upsilon_0/[E]_{tot}$ where υ_0 refers to initial steady-state rates (μM CO oxidized per min) in rate-vs-time plots that lacked lag periods, or to steady-state rates immediately after lag periods, in plots that contained lags. $[E]_{tot}$ in μM were converted from mg/mL values by assuming molecular masses of 62,000 da for each β subunit of $CODH_{Rr}$ (*12*) and 155,000 da for each αβ dimer of $CODH_{Mt}$ (*13*).

Experiment of Figure 2: Effect of Sulfide with $CODH_{Rr}$ on CO Oxidation Activity. A 5.0 mM solution of sodium sulfide (Sigma) was prepared in 0.1 N NaOH. A portion of this stock was added to 1.0 mL of $CODH_{Rr}$ (0.38 μM β, final concentration in buffer A, defined as 100 mM MOPS, pH 7.5) such that the final concentration of sulfide was 200 μM. Another portion of the stock solution was diluted 10:1 with buffer A and aliquots were added to $CODH_{Rr}$ as above, resulting in solutions with 5.0, 10, and 20 μM sulfide. A final portion of the stock solution was diluted 100:1 with buffer A, and aliquots were added to $CODH_{Rr}$ as above, resulting in solutions with 0, 0.5, 1.0 and 2.5 μM of sulfide. These 8 solutions of $CODH_{Rr}$/sulfide were incubated 30 min, and then each was loaded into a stopped-flow syringe as described (*10*). The other syringe contained CO oxidation assay buffer (20 mM methyl viologen (MV) in buffer A equilibrated with 1 atm CO). Each solution was assayed for CO oxidation activity one-by-one such that the last of the 8 solutions was assayed ca. 40 min after the first was assayed. Reactions were at 30º C and monitored in PM mode with 0.15 cm pathlength at 578 nm (ε = 9.8 $mM^{-1}cm^{-1}$). As a result of stopped-flow mixing, final concentrations of sulfide, $CODH_{Rr}$ and MV are half of those in pre-mixed solutions.

Experiments of Figures 3 and 4: EPR Studies. $CODH_{Mt}$ was freed of dithionite by passage through a column of 1.6 × 30 cm Sephadex G-25 equilibrated in buffer B (50 mM Tris-HCl buffer pH 8), then concentrated with a centricon (YM50, Millipore) and transferred to a quartz UV-vis cuvette. While monitoring at 600 nm, sufficient 1.0 mM thionin in Buffer B was added to cause the absorbance to increase (due to unreacted oxidized thionin). The protein was removed from the cuvette, concentrated using a centricon and separated into ten 130 μL aliquots of $CODH_{Mt}$. One aliquot was mixed with 120 μL of buffer B and transferred to an EPR tube, affording sample *a* (final volume, 250 μL). A 100 mM stock solution of sodium sulfide in 0.1 N NaOH was prepared. Two other $CODH_{Mt}$ aliquots were mixed with 12.5 and 25 μL of the stock sulfide solution and with 107.5 and 95 μL of buffer B, respectively, and then transferred to EPR tubes to afford samples *h* and *i*, respectively. A portion of the stock solution was diluted 10:1 with buffer B, and 12.5 and 25 μL were used in preparing samples *f* and *g*. Another portion of stock solution was diluted 100:1, and 0.25, 2.5, 12.5, and 25 μL were used to prepare samples *b*, *c*, *d* and *e*. A 50 mM solution of dithionite in 0.1 N NaOH was freshly prepared, and 10 μL were mixed with the last $CODH_{Mt}$ aliquot and 85 μL Buffer B. After 20 min incubation, 25 μL of the 10:1 diluted sulfide solution was added, affording the 250 μL EPR sample of Figure 4. All samples were incubated for *ca*. 30 min after sulfide was added, sealed with rubber septa, removed from the box and frozen immediately in LN_2.

Experiment of Figure 5: Effect of Sulfide with $CODH_{Mt}$ on CO Oxidation Activity. A 100 mM stock solution of sodium sulfide was prepared in 0.1 N NaOH. A portion of this stock was diluted 10:1 with buffer B and 6 – 240 μL aliquots were mixed with 1074 – 840 μL of buffer B and 120 μL of $CODH_{Mt}$ (35 nM αβ after mixing), resulting in 1.2 mL solutions with 50, 100, 200, 500, 1000 and 2000 μM sulfide. Another portion of the stock was diluted 100:1 with buffer B and

0 – 12 μL aliquots were added to 1068 – 1080 μL of buffer B and 120 μL of $CODH_{Mt}$, resulting in solutions with 0, 5.0 and 10 μM sulfide. After *ca*. 30 min incubation, the resulting 9 solutions were assayed for CO oxidation activity as in the Figure 2 experiment except that the CO oxidation assay solution contained buffer B rather than buffer A, and reactions were monitored at 604 nm ($\varepsilon = 13.9\ mM^{-1}cm^{-1}$) with a 1 cm pathlength.

Experiment of Figure 6: Irrelevance of Pre-Incubation on Sulfide Inhibition. A 60 mL Wheaton vial was sealed with a rubber septum in the glove box and its Ar atmosphere was replaced with 1 atm CO using a Schlenk line. After returning the vial into the glove box, 4.0 mL of buffer A containing 35 nM αβ $CODH_{Mt}$ and 10 μM MV were injected into the vial. The contents were incubated for 5 min, and then 0.8 mL of the resulting CO-saturated solution was loaded into the stopped-flow drive syringe A as described (*10*). Syringe B was loaded with a freshly prepared solution of 2 mM sodium sulfide in buffer A. This solution had been prepared by mixing 40 μL of a 100 mM sodium sulfide plus 100 mM NaOH solution into 1960 μL of buffer A. In the control experiment, syringe B was filled with buffer A alone. Syringe C was loaded with 20 mM MV in buffer A. In the control experiment, syringes A and B were mixed for 0.015 sec and then reacted with syringe C. In the other experiments, syringes A and (sulfide-containing) syringe B were mixed for 0.015, 60 and 500 s before reacting with syringe C. After all mixings, $[CODH_{Mt}]$ = 8.7 nM, [CO] = 220 μM, [MV] = 10 mM, and $[HS^-]$ = 500 μM. CO oxidation activity assays were performed at 30^oC and monitored at 604 nm.

Reversibility of Sulfide Inhibition. An aliquot of $CODH_{Mt}$ (10 μL of 84 μM αβ) was assayed as in the Figure 5 experiment, while the remainder (1.0 mL) was mixed with 10 μL of a freshly-prepared 600 mM stock solution of sodium sulfide in 0.1 N NaOH. After incubating for 40 min, a

10 μL aliquot of the resulting $CODH_{Mt}$ solution with 6.0 mM sulfide was assayed for activity. The remaining solution was divided into two 0.5 mL portions, one of which was reacted with 2 μL of 40 mM freshly-made dithionite, the other of which was exposed to 1 atm CO. After incubating both for 1 hr, solutions were passed individually through columns of Sephadex G25 (1 × 15 cm for the CO-containing sample and 1 × 30 cm for the dithionite-containing sample) that were equilibrated in buffer B. Eluted protein solutions were assayed as in the Figure 5 experiment.

Sample *g* from the EPR experiment of Figure 3 was thawed in the glove box and mixed with 10 μL of 50 mM freshly prepared dithionite. After incubating 30 min, the result solution was passed through a 1 × 15 cm Sephadex G-25 column equilibrated in buffer B. The eluted solution was transferred into a quartz cuvette and titrated with 1 mM thionin as described for the experiment of Figure 3. The thionin-oxidized sample was concentrated to 250 μL with a centricon unit, transferred to a clean EPR tube, sealed with a rubber septum, removed from the box and frozen immediately with LN_2.

Experiment of Figure 7: Effect of CO on Enzyme Stability. A 350 μL stock solution of 16.3 mg/mL $CODH_{Mt}$ was separated into 7 × 50 μL aliquots and transferred into glass tubes (5 × 45 mm, Fisher). Tubes were sealed with rubber septa (which had been stored in the box for > 1 month), then removed from the box. On a Schlenk line with needle outputs, tube headspaces were replaced with 1 atm of pre-purified-grade CO which had been scrubbed for O_2 using an Oxisorb® (Messer) cartridge. Septa were wrapped tightly with electronic tape; then tubes were transferred to an Ar-atmosphere glove box (MBraun, Inc) maintained at 4º C and at < 1 ppm O_2. As a control, 200 μL of the stock solution was transferred into a similar tube and sealed with a septum (i.e. with an Ar headspace). At time t = 0, aliquots of the control and 1 CO-treated sample were removed from the box and assayed for CO oxidation activity as described (*11*). Similar assays were

performed at various times, using a different CO-treated aliquot at each time (minimizing CO leakage caused by punctured septa). After t = 664 hrs, 20 μL of assay buffer without CO (50 mM Tris plus 20 mM MV^{2+}) was injected into the CO-treated sample which had been assayed at t = 0. The solution immediately turned dark blue, indicating the presence of CO in that sample 664 hrs after it was prepared. In contrast, the Ar-treated control showed no evidence of turning blue indicating the absence of CO in the control sample 664 hrs after it was prepared.

Results

Adding sodium sulfide to $CODH_{Rr}$ attenuated steady-state CO oxidation activity (Figure 2). Although there are multiple equilibria involving sulfide ions in aqueous solution at neutral pH, with HS^- the predominant species (*14*), we will refer to all species collectively as *sulfide* ions. Activities declined with increasing amounts of added sulfide ion, but not to zero activity even at the highest concentrations used. In the absence of sulfide, no lag phase was evident. Electrochemical potentials of the $CODH_{Rr}$ solutions used in these experiments ranged from -210 mV to -310 mV vs. NHE. These potentials and the absence of a lag phase are consistent with the C-clusters in these $CODH_{Rr}$ samples being in the C_{red1} state at the time of injection (*10*). Equivalent samples to which sodium sulfide was added exhibited a lag phase. The length of this lag increased with increasing sulfide ion concentration, reaching a maximum of ~ ½ sec.

Samples of $CODH_{Mt}$ were freed from dithionite and oxidized with a slight excess of thionin. In this state only the g_{av} = 1.82 signal from the C_{red1} state was evident in EPR spectra (Figure 3, Panel B, spectrum *a*). Adding increasing amounts of sulfide caused the g_{av} = 1.82 signal to decline and a new rather complex set of spectral features to develop (Figure 3, Panel A; Panel B, spectra *f* – *i*; Panel C; Panel D). The similarity of these features to the g_{av} = 1.82 signal, in terms of g-values and temperature and power dependences, suggests that some or all of these features

originate from the C-cluster (possibly in various conformations). The dominant signal appears to have g-values of 1.95, 1.85, and (1.70 or 1.62), as is most clearly discerned from the spectrum obtained at 4 K and 20 mW (Panel D, spectra *a*) where some of the minor features have saturated. At 16 K, contributions from B_{red} are apparent, as the signals originating from the C-cluster broadened beyond detection. Taken together, these changes indicate that sulfide binds to the C-cluster in the C_{red1} state. Another sample of $CODH_{Mt}$ was reduced with CO, affording the g_{av} = 1.86 signal from the C_{red2} state. Addition of sulfide to a matched sample had no effect on this signal (Figure 4). Thus, it would appear that sulfide does not bind to the C-cluster in the C_{red2} state.

Since the EPR experiments were performed with $CODH_{Mt}$, we thought it pertinent to examine the CO oxidation activity of $CODH_{Mt}$ in the presence of increasing concentrations of sulfide (Figure 5 and Table 1). Behavior was similar to that of $CODH_{Rr}$, in that sulfide inhibited catalysis without causing complete inhibition even at the highest concentrations used. Unlike the situation with $CODH_{Rr}$, no lags were observed when $CODH_{Mt}$ was used.

To examine whether the effects of sulfide were reversible, a sample of $CODH_{Mt}$ was assayed for activity (measured to be 9,100 min^{-1}), then incubated with sulfide and re-assayed. The resulting activity corresponded to 62% of the control activity. Efforts were made to remove the added sulfide, by reduction (using CO and dithionite) and passage through a chromatography column commonly used to remove small molecules from proteins. After this procedure, the CO-treated sample had an activity corresponding to 95% of the control, while the dithionite-treated sample had an activity corresponding to 88% of the control. We conclude that the inhibitory effect of sulfide is reversible under reducing conditions. A related experiment was monitored by EPR. In this case, the g_{av} = 1.82 signal returned after similar efforts were taken to remove sulfide.

We were initially under the impression that pre-incubating the enzyme with sulfide was required for inhibition to be observed. To examine this systematically, sulfide was mixed with MV-reduced $CODH_{Mt}$ for 0.015, 60 and 500 sec (Figure 6). Relative to the control experiment (lacking sulfide, Figure 6A), the extent of inhibition was 69%, 66%, and 66%, respectively. These experiments show that pre-incubation is not required for inhibition of CO oxidation activity by sulfide.

For reasons that will become apparent in the *Discussion* section, a sample of $CODH_{Mt}$ was divided into aliquots; one was incubated under an Ar atmosphere and 7 under CO. All aliquots were stored anaerobically and then assayed periodically for CO oxidation activity over the course of 664 hrs. Both groups retained ~80% of initial activity (Figure 7). If the first data points acquired immediately after setting up the experiment are ignored, *no* loss of activity in either sample is evident during the following 652 hr period. We conclude that the structure of the catalytically active C-cluster is unaffected by the presence of CO - i.e. CO does not react with the enzyme and thereby inactive it.

Analysis

Results of the experiment shown in Figure 2 suggest that $CODH_{Rr}$ binds sulfide ion in one intermediate state of catalysis and then expels it when the enzyme progresses into another such state. An alternative interpretation is that $CODH_{Rr}$ slowly catalyzes the oxidation of CO with sulfide ion bound. However, the presence of a lag phase prior to the onset of catalysis and the non-zero steady-state activity ultimately achieved discount this possibility. The lag phase indicates that sulfide binds to the enzyme *prior* to catalysis (during pre-incubation) in a manner that is completely inhibitory. The EPR experiments of Figures 3 and 4 indicate that sulfide binds to the C_{red1} state but not to the C_{red2} state. The non-zero steady-state activities which were eventually

established in the experiment of Figure 2 indicate that the general population of inhibited enzyme molecules (in what we call the C_{red1}:S state) somehow activate by dissociating sulfide. The fact that post-lag steady-state activities in the presence of sulfide were *less* than in assays lacking sulfide ion suggests that the inhibitor sulfide associates with and dissociates from the enzyme during each catalytic turnover.

A simple model rationalizing this behavior is shown in Figure 8. Accordingly, the C-cluster cycles between C_{red1} and C_{red2} during catalysis. The C_{red1} state has an hydroxyl group bound, and this group is displaced when sulfide ion binds to the C_{red1} state. Sulfide ion binding to C_{red1} occurs reversibly but sulfide does not bind to the C_{red2} state. The sulfide-bound [Ni^{2+}-HS^--Fe^{2+}] state (C_{red1}:S) can be reduced to yield C_{red2} and free sulfide ion. Without this last assumption, the observed residual activity in the presence of excess sulfide ion could not be explained simply.

The model can be simplified further and used to analyze our data by assuming that [CO], [OH^-], [H^+] and [MV^{2+}] are invariant during the reaction. If the measured product of catalysis is called "P" rather than $2MV^{1+}$, the model becomes reactions [2] – [6].

$$C_{red1} \xrightarrow{k_1} C_{red2} \qquad [2]$$

$$C_{red2} \xrightarrow{k_2} C_{red1} + P \qquad [3]$$

$$C_{red1} + HS^- \xrightarrow{k_3} C_{red1}{:}S \qquad [4]$$

$$C_{red1}{:}S \xrightarrow{k_4} C_{red1} + HS^- \qquad [5]$$

$$C_{red1}{:}S \xrightarrow{k_5} C_{red2} + HS^- \qquad [6]$$

The differential equations for $\frac{d[C_{red1}]}{dt}, \frac{d[C_{red2}]}{dt}, and \frac{d[C_{red1}:S]}{dt}$ as generated from these reactions were equated to zero according to the steady-state assumption and solved for C_{red2} using relationship $[C_{red1}:S] = [C_{tot}] - [C_{red1}] - [C_{red2}]$. The reaction velocity at steady state is

$$\upsilon = \frac{d[P]}{dt} = k_2[C_{red2}] = \frac{k_2(k_1k_4 + k_3k_5[HS^-] + k_1k_5)[C_{tot}]}{k_1k_4 + k_1k_5 + k_2k_4 + k_3k_5[HS^-] + k_2k_3[HS^-] + k_2k_5} \quad [7].$$

In the absence of sulfide ion, $[HS^-] = 0$ and [7] becomes

$$\upsilon_{max} = \frac{k_1k_2[C_{tot}]}{k_1 + k_2} \quad [8]$$

while in the limit as $[HS^-]$ approaches infinity, [7] becomes

$$\upsilon_{min} = \frac{k_2k_5[C_{tot}]}{k_2 + k_5} \quad [9].$$

From the data of Table 1, υ_{max} = 102,900 min^{-1}, υ_{min} = 39,900 min^{-1}, and $[C_{tot}]$= 0.19 μM.

Substituting these values into [8] and [9], and solving for k_1 and k_5 yields

$$k_1 = \frac{10290000k_2}{19k_2 - 10290000} \text{ and } k_5 = \frac{210000k_2}{k_2 - 210000}. \quad [10,11]$$

The sulfide concentration which yielded the reaction velocity midway between υ_{max} and υ_{min} was equated to the apparent dissociation constant K_I for sulfide binding, yielding

$$K_I = [HS^-]_{\left(at\, v = \frac{v_{max} + v_{min}}{2}\right)} = \frac{k_1k_4 + k_1k_5 + k_2k_4 + k_2k_5}{k_3(k_2 + k_5)} \quad [12].$$

Substituting this relationship, as well as those for k_1 and k_5 into [7] yields

$$\upsilon = \frac{102900K_I + 39900[HS^-]}{K_I + [HS^-]} \quad [13].$$

Pairs of values $\{\upsilon, [HS^-]\}$ given in Table 1 were substituted into [13] and the resulting relationships were solved for K_I, yielding the average value 40 ± 10 nM.

Applying the same model to $CODH_{Mt}$ and analysis as was used for $CODH_{Rr}$ afforded the rate equation

$$\upsilon = \frac{8750K_I + 5190[HS^-]}{K_I + [HS^-]} \qquad [14].$$

The value of K_I was again adjusted to fit the data of Table 1, yielding $K_I = 60 \pm 30$ μM. Thus, sulfide ion binds more tightly to $CODH_{Rr}$ than it does to $CODH_{Mt}$. This difference in binding strength may explain the absence of a lag phase in the $CODH_{Mt}$ experiment. It is also congruent with the somewhat higher concentrations of sulfide required for there to be noticeable effects in $CODH_{Mt}$ EPR spectra than were required to observe effects in activity of $CODH_{Rr}$.

Discussion

It is simplest to assume that sulfide ion inhibits CO oxidation catalysis by binding to the C-cluster in the manner evident in the structure of Dobbek et al. (*2*) – i.e. bridging the Ni and the unique Fe (Figure 1, left-hand side). The ability of sulfide to bind to the C_{red1} state but not to C_{red2} suggests that $CODH_{Ch}$ may have been crystallized in the $C_{red1}S$ state (or in the C_{ox} or C_{int} states, as we have no information as to whether sulfide binds these states of the C-cluster), and that the other structures may have been crystallized in more reduced states such as C_{red2}. Given our evidence that sulfide ion is a dissociable inhibitor, the intrinsic structure of the C-cluster would be that of Figure 1, right-hand side.

The effect of sulfide ion on CODH activity and spectral properties are qualitatively similar to those of other anions, including cyanide, cyanate, thiocyanate, and azide ions (*15-17*). Cyanide ion fully inhibits CODH's, apparently by binding to the C_{red1} state as evidenced by a shift in the C_{red1} EPR signal when CN^- is added (*15*). This effect can be reversed (i.e. activity recovers fully and the EPR signal converts to that from C_{red2}) when CN^--treated enzyme is incubated in CO for *ca.* 1 hr. Also, pre-treatment with CO protects the enzyme from the effects of CN^-, apparently by

maintaining it in the C_{red2} state. Thus, it appears that this anion does not bind to the C_{red2} state. Thiocyanate, cyanate and azide also appear to bind C_{red1} but not C_{red2} (*16-17*). Similar to sulfide, inhibition by thiocyanate is partial (*16*). This reactivity pattern common to sulfide and other inhibitory anions suggests that these other anions might also bind to the enzyme in the same manner as sulfide – i.e. bridging the Ni and unique Fe of the C-cluster.

Binding of CN^- shifts the position of Ferrous Component II in Mössbauer spectra (*8*) which corresponds to the unique Fe of the C-cluster. This suggests that CN^- binds to the unique Fe; whether it also binds, in bridging fashion, to the Ni would not have been evident from the Mössbauer experiments. With CN^- bound, added CO cannot reduce the enzyme's Fe-S clusters, suggesting that CO does not oxidize to CO_2 when CN^- is bound. Nevertheless, CO incubation can (somehow) accelerate the dissociation of CN^- (*15*). One possibility is that CO binds to the C-cluster in the C_{red1} state with CN^- bound simultaneously, and that this binding encourages CN^- dissociation (*15,18*). Initially, CO was thought to reactivate CN^--inhibited CODHs noncompetitively by binding to a "modulator" site that was distinct from the C-cluster (*15*). However, once it was understood that the C-cluster's spin density resided predominately on the Fe-S portion of the C-cluster rather than on the Ni, the modulator was proposed to be the Ni itself (*7*). The presumed bridging mode for CN^- binding helps explain how CO binding to Ni might accelerate CN^- dissociation, in that CO binding might weaken Ni coordination to CN^- such that CN^- would become bound only to the unique Fe.

Using ENDOR spectroscopy, DeRose *et al.* (*19*) identified a strongly coupled proton associated with the C_{red1} state (but not with C_{red2}) that was displaced by CN^-. Interpreting the proton as arising from the substrate hydroxide, this suggests that CN^- and OH^- bind at the same site. We were initially opposed to the idea that hydroxide bridges the Ni and unique Fe, because such binding would *deactivate* it in terms of nucleophilicity. However, such a bridging

arrangement might also be required to deprotonate water at the appropriate pK_a for this reaction (i.e. coordination to Fe alone might not lower the pK_a sufficiently) or it might facilitate OH^- dissociation. A similar situation (water bridging two metal centers followed by deprotonation and nucleophilic attack) is evident in the enzyme arginase (*20*). In this case, the hydroxide ion bridging two Mn(II) ions is an effective nucleophile for the hydrolysis reaction.

The connection between inhibitory anions and the substrate hydroxyl group suggests that they might bind similarly and share additional reactivity properties. Firstly, hydroxide might also bind to C_{red1} (or more accurately, bind to an unnamed state of the C-cluster that becomes C_{red1} once the hydroxide is bound) but not to C_{red2}, as supported by the ENDOR study. Secondly, CO binding may promote the dissociation of bound OH^- similarly to the way it promotes the dissociation of bound CN^-. This situation is depicted in Figure 9. Here, water binds in bridging mode to the Ni and unique Fe of the C_{red1} state. This lowers the pK_a of the water to the value observed – namely 7.2 (*16*) and results in a bridging hydroxyl group. When CO binds to the Ni, the Ni-OH bond breaks and a terminally-bound HO-Fe species is formed. This weakly-bound terminal hydroxyl group then dissociates from the Fe and attacks the carbonyl of Ni-bound CO. Thus, *CO-induced labilization might serve to increase the nucleophilic propensity of the hydroxyl group*. We find this an intriguing possibility that deserves further evaluation.

Finally, while this paper was being reviewed, another study was published by Meyer and coworkers in which the sulfide ion bridging the Ni and unique Fe in the $CODH_{Ch}$ C-cluster was concluded to be *required* for activity (*21*). This conclusion was based on a correlation between the presence/absence of this sulfide in X-ray crystal structures and the activity/inactivity of other samples treated similarly. In the presence of CO, their sample lost ~100% activity in ~100 hrs whereas in the absence of CO (under an N_2 atmosphere), ~60% of initial activity remained after the 100 hr incubation. The analogous experiment performed using $CODH_{Mt}$ in our lab afforded

significantly different results (Figure 7) which do not support the conclusion that CODH's are inactivated upon treatment with CO. We suspect that the absence of the bridging sulfide in their CO-treated samples arose because the C-cluster was in the C_{red2} state and would not support sulfide binding. The presence of bridging sulfide in samples prepared in the *absence* of low-potential reductants may have arisen because the C-cluster was in the C_{red1} state, and sufficient sulfide was present to bind and form the C_{red1}:S state. The presence of bridging sulfide in the sample prepared in the *presence* of dithionite is more difficult to explain, in that the C-cluster should have been in the C_{red2} state and unable to bind sulfide. However, $CODH_{Mt}$ consumes dithionite spontaneously (*11*) raising the possibility that the dithionite-reduced sample was more oxidized than expected by the time it was exposed to X-rays. Despite differences in interpreting the role of the bridging sulfide in CODH catalysis, the results of Dobbek *et al.* (*21*) support our assumption that the sulfide bridging the Ni and unique Fe of a given C-cluster is labile and can bind/dissociate under appropriate conditions.

Acknowledgement: We thank Juan C. Fontecilla-Camps for suggesting (despite our initial objections) that the hydroxide ion used in catalysis might bridge the Ni and unique Fe of the C-cluster.

Table 1. CO oxidation activities of $CODH_{Rr}$ and $CODH_{Mt}$ (min^{-1}) at various concentrations of sodium sulfide (μM). The concentrations of $CODH_{Rr}$ and $CODH_{Mt}$ after mixing were 190 nM β and 17.5 nM αβ, respectively. Reaction rates were determined from the linear regions shown in Figure 2 for $CODH_{Rr}$ (and not shown for $CODH_{Mt}$).

$CODH_{Rr}$		$CODH_{Mt}$	
$[HS^-]$	CO oxidation activity	$[HS^-]$	CO oxidation activity
0	102,900	0	8,750
0.25	51,500	2.5	8,400
0.50	47,100	5.0	8,100
1.25	41,350	25	7,550
2.50	40,950	50	7,000
5.00	39,950	100	7,050
10.0	40,100	250	5,900
100	39,900	500	5,650
		1000	5,500

Figure Legends

Figure 1. C-Cluster Structures. The structure on the left was reported for $CODH_{Ch}$ (*2*) while that on the right represents those structure reported for $CODH_{Mt}$ and $CODH_{Rr}$ (*3*, *4*, *5*). Other differences between the four structures are not highlighted.

Figure 2. CO Oxidation Activity of $CODH_{Rr}$ in the Presence of Sodium Sulfide. Assays were performed as described in *Experimental Procedures*. Final concentrations of sulfide ion (in μM) were: *A*, 0; *B*, 0.25; *C*, 0.5; *D*, 1.25; *E*, 2.5; *F*, 5; *G*, 10; *H*, 100. Displayed traces are the average of three experimental traces. Each trace began at ca. 0.02 AU. Traces *B* – *H* are offset by 0.1 AU increments in the figure.

Figure 3. Effect of Sodium Sulfide on C_{red1} EPR Spectra from $CODH_{Mt}$. $CODH_{Mt}$ (130 μM αβ poised with the C-cluster in the C_{red1} state as described in *Experimental Procedures*) was treated with sodium sulfide at the following concentrations (in μM). Panel A, 10,000; Panel B, *a*) 0; *b*) 1; *c*) 10; *d*) 50; *e*) 100; *f*) 500; *g*) 1000; *h*) 5000; *i*) 10,000 (same sample as for Panel A). EPR conditions: Modulation amplitude, 10 G; microwave frequency, 9.600 GHz; microwave power, 20 mW; dual-mode cavity; temperature, 10 K. Panel C, same as trace *g* Panel B, showing close up of minority features. Panel D, same as in Panel C, but obtained at 4 K and 16 K. EPR conditions as above except that the microwave frequency was 9.450 GHz and the standard cavity was used.

Figure 4. EPR Spectrum of $CODH_{Mt}$ Poised in the C_{red2} State. Sodium sulfide was 1 mM. Refer to Figure 7B of (*7*) for a control C_{red2} spectrum. EPR conditions were as in Figure 3, Panel B.

Figure 5. CO Oxidation Activity of $CODH_{Mt}$ Pre-Incubated in Sodium Sulfide. Assays were performed as described in *Experimental Procedures*. Final concentrations of sulfide ion (in μM) were 0, 2.5, 5, 25, 50, 100, 250, 500, 1000. Activities are given in Table 1 and the solid line is a simulation using equation [14] with K_I = 60 μM. Reaction rates were determined from the linear regions of absorbance traces, including 4 – 4.5 sec for 0, 2.5, 5, 25, 50, 100 μM samples, and 19 – 20 sec for 250, 500, 1000 μM samples.

Figure 6. Stopped-flow traces showing the irrelevance of pre-incubation on sulfide inhibition. See *Experimental Procedures* for details. Incubation times: A, no sulfide present; B, 0.015 sec; C, 60 sec; D, 500 sec. Traces have been shifted from each other by 0.1 absorbance units for clarity.

Figure 7. Effect of Incubating CO with $CODH_{Mt}$ on CO Oxidation Activities. Triangles, $CODH_{Mt}$ in 1 atm CO (initial activity = 16,500 min^{-1}). Circles, $CODH_{Mt}$ in 1 atm Ar (initial activity = 14,400 min^{-1}). See *Experimental Procedures* for details. Percentage of activity plotted is relative to control activity at t = 0.

Figure 8. Model for Sulfide Inhibition. See text for details.

Figure 9. Mechanism of catalysis, emphasizing a proposed μ^2-bridging Hydroxyl Group and CO-Induced Labilization. See text for details.

References

1. Lindahl, P. A. (2002) *Biochemistry 41*, 2097-2105.

2. Dobbek H., Svetlitchnyi, V., Gremer, L., Huber, R., Meyer, O. (2001) *Science 293*, 1281-1285.

3. Drennan, C. L., Heo, J., Sintchak, M.D., Schreiter, E., Ludden, P.W. (2001) *Proc. Natl. Acad. Sci. USA*. *98*, 11973-11978.

4. Doukov, T.L., Iverson, T.M., Saravalli, J., Ragsdale, S.W., Drennan, C.L. (2002) *Science 298*, 567-572.

5. Darnault, C, Volbeda A, Kim E.J., Legrand P., Vernede X., Lindahl P.A., Fontecilla-Camps J.C. (2003) *Nature Structural Biology 10*, 271-279.

6. Lindahl, P.A., Münck, E., Ragsdale, S.W. (1990) *J. Biol. Chem. 265*, 3873 - 3879.

7. Anderson, M.E., Lindahl, P.A. (1996) *Biochemistry 35*, 8371-8380.

8. Hu, Z., Spangler, N. J., Anderson, M. E., Xia, J. Q., Ludden, P. W., Lindahl, P.A., Münck, E. (1996) *J. Am. Chem. Soc*. *118*, 830 - 845.

9. Fraser, D.M., Lindahl, P.A. (1999) *Biochemistry, 38*, 15706-15711.

10. Feng, J., Lindahl P.A. (2004) *Biochemistry, 43*, 1552-1559.

11. Shin, W., Stafford, P.R., Lindahl, P. A. (1992) *Biochemistry 31*, 6003-6011.

12. Bonam, D., Ludden, P.W. (1987) *J. Biol. Chem*. *262*, 2980-2987.

13. Morton, T.A., Runquist, J.A., Ragsdale, S.W., Shanmugasundaram, T., Wood, H.G., Ljungdahl, L.G. (1991) *J. Biol. Chem.* 266, 23824-23828.

14. Weast, R.C., ed. (1986) Handbook of Chemistry and Physics, 66th edition, CRC Press, Boca Raton, FL. The predominance of HS^- is evident by applying the pK's of H_2S given in this reference (7.04 and 11.96) to the Henderson-Hasselbalch equation.

15. Anderson, M.E., Lindahl, P.A. (1994) *Biochemistry 33*, 8702 - 8711.

16. Seravalli, J., Kumar, M., Lu, W.P., Ragsdale, S.W. (1995), *Biochemistry 34*, 7879-7888.

17. Seravalli, J., Kumar, M., Lu, W.-P., Ragsdale, S.W. (1997) *Biochemistry 36*, 11241-11251.

18. Anderson, M. E., DeRose, V. J., Hoffman, B. M., Lindahl, P. A. (1993) *J. Am. Chem. Soc. 115*, 12204-12205.

19. DeRose, V. J., Anderson, M. E., Lindahl, P. A., Hoffman, B. M. (1998) *J. Am. Chem. Soc. 120*, 8767 - 8776.

20. Dismukes, G.C. (1996) *Chem. Rev. 96*, 2909-2926.

21. Dobbek, H., Svetlitchnyi, V., Liss, J., Meyer, O. (2004) *J. Am. Chem. Soc. 126*, 5382-5387.

Figure 1

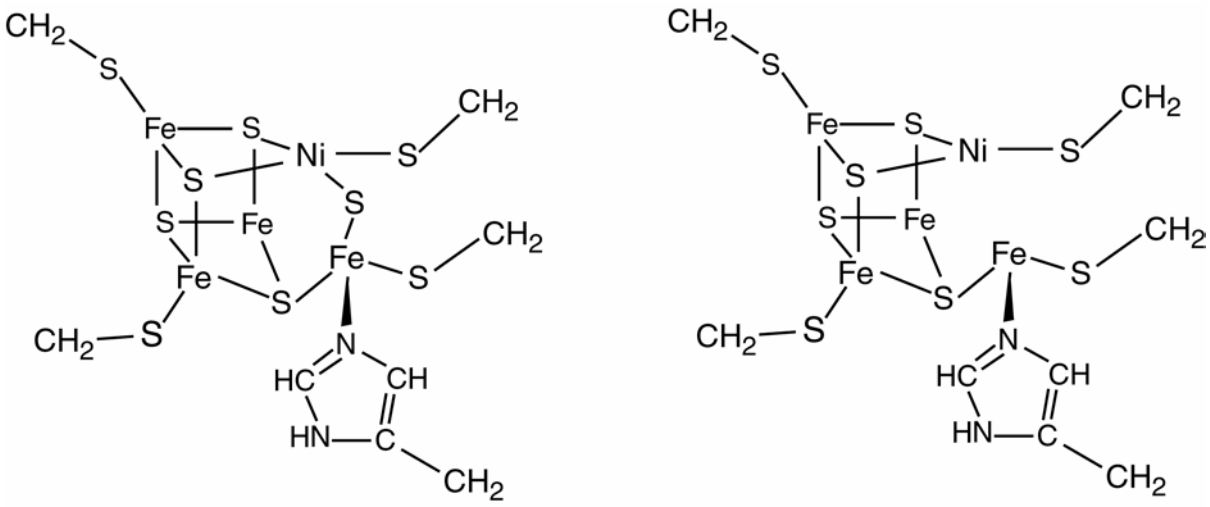

Figure 2

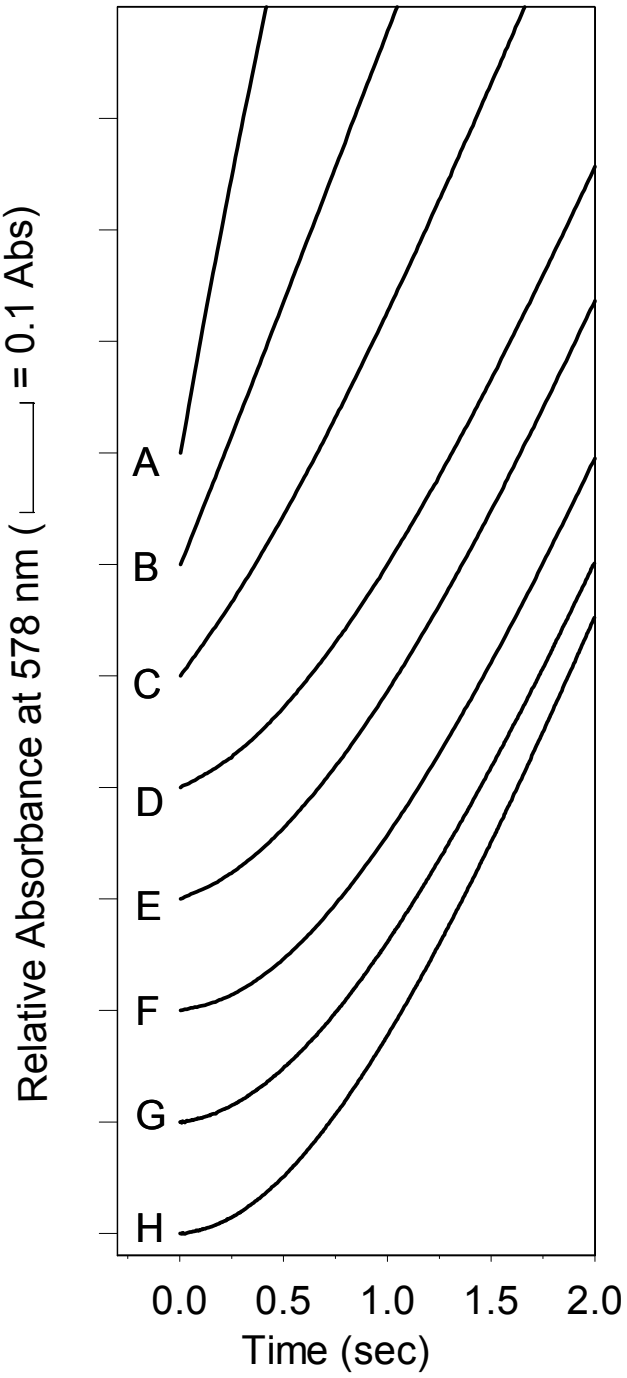
Relative Absorbance at 578 nm (⌊ = 0.1 Abs)
A
B
C
D
E
F
G
H
0.0
0.5
1.0
1.5
2.0
Time (sec)

Figure 3

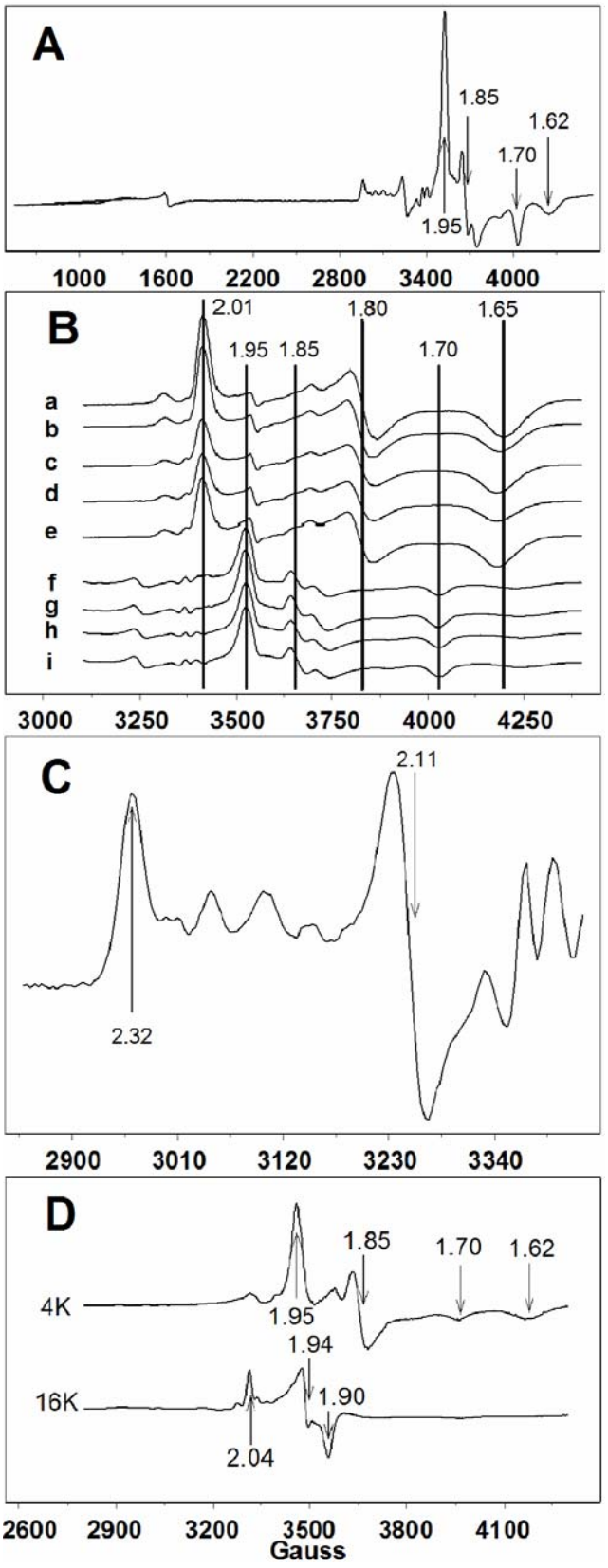
A
1.85
1.62
1.70
1.95
1000 1600 2200 2800 3400 4000
B
2.01
1.80
1.65
1.95 1.85
1.70
a
b
c
d
e
f
g
h
i
3000 3250 3500 3750 4000 4250
C
2.11
2.32
2900 3010 3120 3230 3340
D
1.85
1.70
1.62
4K
1.95
1.94
16K
1.90
2.04
2600 2900 3200 3500 3800 4100
Gauss

Figure 4

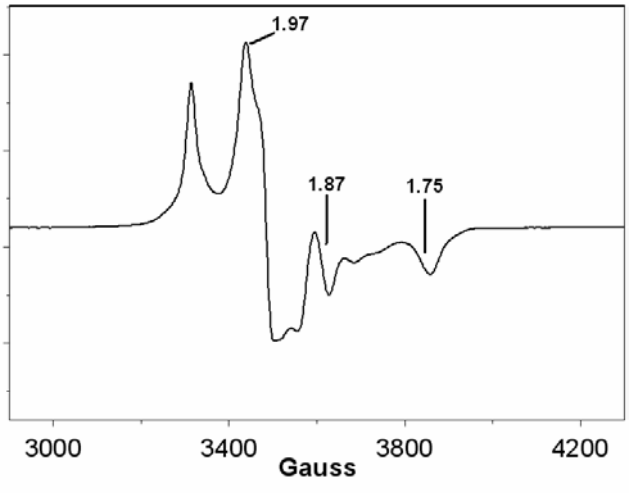

Figure 5

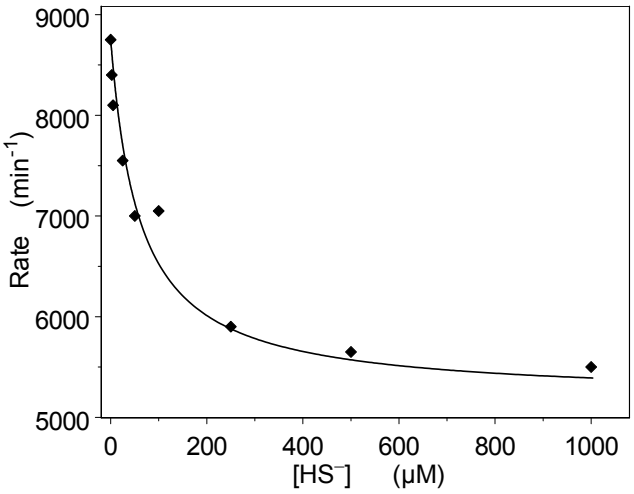

Figure 6.

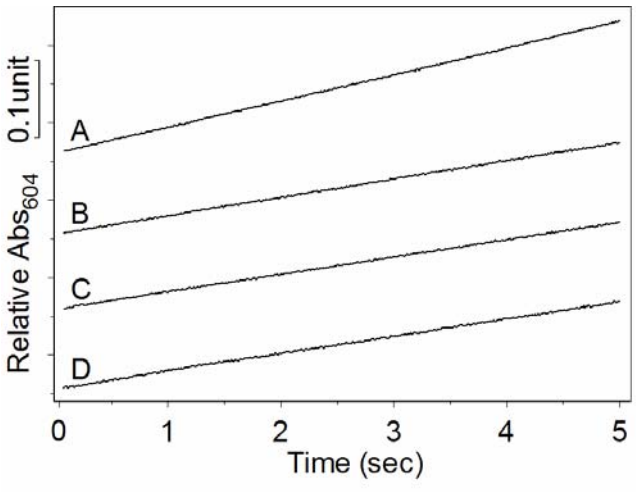

Figure 7.

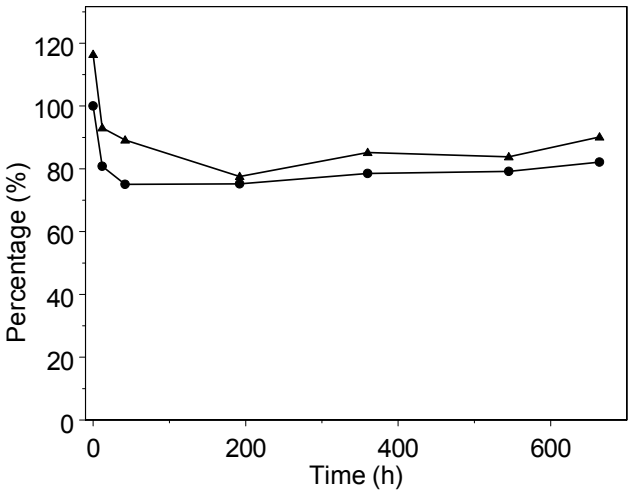

Figure 8

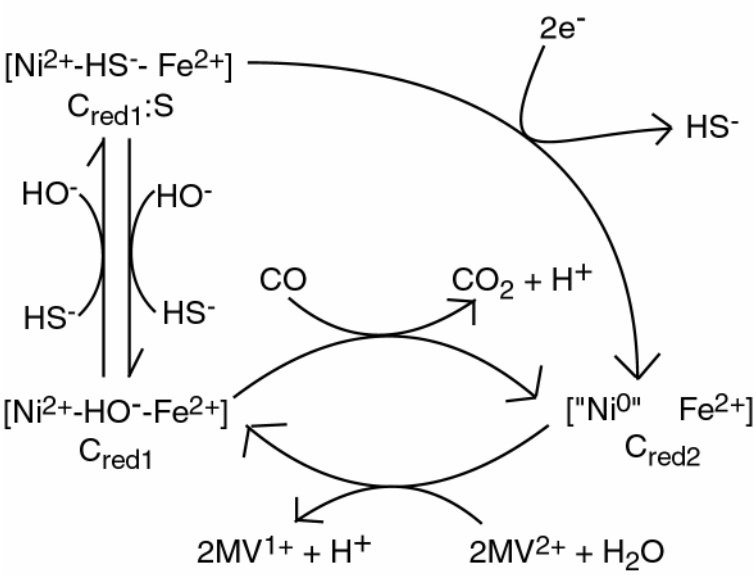
2e-
[Ni2+-HS- Fe2+]
Cred1:S
HS-
HO-
HO-
HS-
HS-
CO
CO2 + H+
[Ni2+-HO--Fe2+]
Cred1
["Ni0" Fe2+]
Cred2
2MV1+ + H+
2MV2+ + H2O

Figure 9.

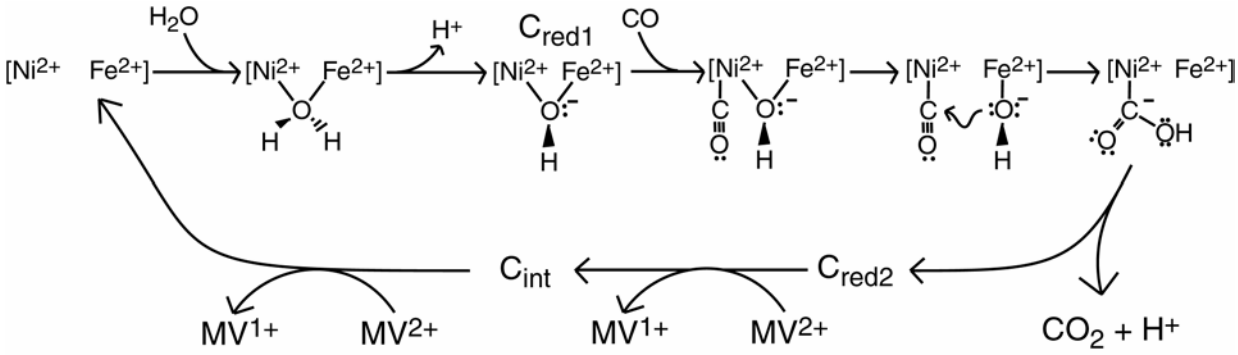
H2O
H+
Cred1
CO
[Ni2+ Fe2+]
[Ni2+ Fe2+]
[Ni2+ Fe2+]
[Ni2+ Fe2+]
[Ni2+ Fe2+]
[Ni2+ Fe2+]
Cint
Cred2
MV1+
MV2+
MV1+
MV2+
CO2 + H+

Table of Contents Graphic: